Eur Biophys J (1992) 20:321–335

European Biophysics Journal

Redox control of proton transfers in membrane b-type cytochromes: an absorption and resonance Raman study on bis(imidazole) and bis(imidazolate) model complexes of iron-protoporphyrin

A. Desbois [1,*] **and M. Lutz** [2]

[1] Laboratoire de Biophysique, Institut de Biologie Physico-Chimique, 13 rue Pierre et Marie Curie, F-75005 Paris, France
[2] Section de Biophysique des Protéines et des Membranes, Département de Biologie Cellulaire et Moléculaire, Unité de Recherche Associée au C.N.R.S. 1290, Centre d'Etudes de Saclay, F-91191 Gif-sur-Yvette Cedex, France

Received July 12, 1991 / Accepted in revised form October 16, 1991

Abstract. Optical absorption spectra and resonance Raman (RR) spectra, obtained with Soret excitation, are reported for bis(imidazole) and bis(imidazolate) complexes of iron(II)- and iron(III)-protoporphyrin IX, prepared in aqueous conditions. Perdeuteration experiments on the axial ligands permitted the assignment of the symmetric Fe-(ligand)$_2$ stretching mode of Fe[x]PP(L)$_2$ to RR bands at 203 (x = II; L = ImH), 212 (x = II; L = Im$^-$), 201 (x = III; L = ImH) and 226 cm^{-1} (x = III; L = Im$^-$). These frequency differences indicate a strengthening of the axial bonds when the imidazole deprotonations occur. The larger difference observed for the ferric derivatives reflects the stronger σ-donor capability of the Im$^-$ anion for iron(III) over iron(II). For the ferrous derivatives, the frequencies of several skeletal porphyrin modes (ν_4, ν_{10}, ν_{11} and ν_{38}) are downshifted by 2–10 cm^{-1} upon deprotonation of the ligands. This effect corresponds to an increased back-bonding from the metal atom to the porphyrin ring when the axial ligand decreases its π-acid strength. Bringing further support to this interpretation, an inverse linear relationship is established between the frequencies of ν(Fe(II)-L$_2$) and ν_{11}. This correlation is expected to monitor the overall H-bonding state of histidine ligands of reduced cytochromes b. On the other hand, absorption measurements have characterized large pK$_a$ differences for the sequential imidazole ionizations of Fe[x]PP(ImH)$_2$ in aqueous cetyltrimethylammonium bromide (9.0 and 10.8 for x = III; 13.0 and 14.1 for x = II). These titrations show that Fe(II)PP(Im$^-$)$_2$ and Fe(III)PP(ImH)$_2$ are good proton-acceptor and proton-donor, respectively, and suggest a model by which heme, located in a favorable environment inside a cytochrome, could couple a cycle of electron transfer with a proton transfer. Based on sequence data and structural models, it is further proposed that, in several membrane cytochromes b (b, b_6, b_{559}), a positively charged amino acid residue and an imidazolate ligand of the ferriheme could form an ion pair involved in a redox control of proton transfer.

Key words: Ligand deprotonation – Iron-ligand modes – Porphyrin modes – Proton transfer

Introduction

The redox potentials of cytochromes vary from −400 to +400 mV. The inductive effects of the heme-side chains, the axial ligand composition and the hydrophobicity of the heme environment are the main factors contributing to this wide range of potentials (Falk 1964; Harbury et al. 1965; Kassner 1972; Stellwagen 1978). Beside these factors, more subtle effects concern the state of the axial histidylimidazole(s) which constitute heme ligand(s) in a very large majority of cytochromes. In all hemoproteins of this class for which crystallographic structures are available, the metal-bound histidylimidazole ring is found to be hydrogen bonded to an electronegative group of the polypeptide chain (Mathews et al. 1972a, b; Salemme et al. 1973; Takano and Dickerson 1981; Pierrot et al. 1982). The possibility that this hydrogen bond might play a functional role has been proposed by Peisach and coworkers (Peisach et al. 1973; Peisach and Mims 1977) and, later, by Valentine and coworkers (Valentine et al. 1979; Swartz et al. 1979). In particular, the influence of the hydrogen bond on histidylimidazole has been invoked as inducing a differential stabilization of oxidation states of cytochromes (Valentine et al. 1979). However, this effect cannot be evaluated without knowledge about the elec-

* *Present address and address for offprint requests:* Section de Biophysique des Protéines et des Membranes, Département de Biologie Cellulaire et Moléculaire, Unité de Recherche Associée au C.N.R.S. 1290, Centre d'Etudes de Saclay, F-91191 Gif-sur-Yvette Cedex, France

Abbreviations: RR, resonance Raman; EPR, electron paramagnetic resonance; PP, protoporphyrin IX; ImH, imidazole; Im$^-$, imidazolate; Im*, imidazole or imidazolate; 1MeIm, 1-methylimidazole; HisH, histidine; His$^-$, histidinate; CTABr, cetyltrimethylammonium bromide; NaDS, sodium dodecylsulphate; VLP, very low potential; LP, low potential; HP, high potential

tronic and structural consequences of this interaction at the porphyrin macrocycle and at its axial bonds.

Resonance Raman (RR) spectroscopy is one of the most powerful techniques for characterizing heme structures and environments of hemoproteins and model compounds (Spiro 1985; Kitagawa and Ozaki 1987; Desbois et al. 1984b, 1989). Thus, among several possible approaches to the study of the H-bonding effects at the coordinated ligands, we have undertaken a RR investigation on bis(imidazole) and bis(imidazolate) complexes of heme. Although a total deprotonation of histidylimidazole has not yet been clearly characterized in a functional cytochrome, imidazolate (Im^-) is in fact generally considered as the limiting form of a very strong hydrogen bonding at imidazole (ImH) (Nappa et al. 1977). In view of these considerations, the present paper reports a detailed spectroscopic investigation (electronic absorption and resonance Raman) of bis(imidazole) and bis(imidazolate) complexes of iron(II)- and iron(III)-protoporphyrin in various aqueous conditions. This study should be of particular relevance in the interpretation of spectral data concerning *b*-type cytochromes in which the protoheme(s) is (are) coordinated by two histidylimidazole ligands.

Materials and methods

Protohemin (Sigma type I) dissolved in aqueous alkaline solution has been used throughout as a starting material. The bis(imidazole) complex of iron(III)-protoporphyrin [Fe(III)PP$(ImH)_2$] was prepared by addition of an excess of imidazole (Desbois and Lutz 1981). In order to avoid porphyrin aggregation, a cationic (cetyltrimethylammonium bromide, Sigma) or an anionic (sodium dodecylsulphate, BDH) detergent was added at a micelle-forming concentration (2% [w/v]). The bis(imidazolate) complex of Fe(III)PP was obtained by alkaline titration of Fe(III)PP$(ImH)_2$ in aqueous CTABr solutions with sodium or potassium hydroxide (see also Results and Discussion). In order to form the ferrous derivatives, heme reduction was achieved by addition, under vacuum, of solid dithionite contained in a side arm of the Raman cell (Desbois and Lutz 1981; Desbois et al. 1984a).

Perdeuterated imidazole (d_3-ImD) (isotopic enrichment: 98.8%), D_2O (isotopic enrichment: 99.8%), DCl (isotopic enrichment: 99.5%, 7.6 N in D_2O) and NaOD (isotopic enrichment: 98.5%, 9.8 N in D_2O) were purchased from the Bureau des Isotopes Stables of the Centre d'Etudes Nucléaires de Saclay.

The Raman spectra were obtained using equipment described previously (Desbois et al. 1979, 1989). Samples were excited with 413.1 nm (Coherent Innova Kr^+), 441.6 nm (Liconix He-Cd) and/or 454.5 nm (Coherent Innova Ar^+) laser beam(s), with radiant powers of 40–60 mW. Improvement in signal to noise ratios of the resonance Raman spectra was achieved by summation of 4–20 scans using a multichannel analyser (Tracor Northern TN 1710). Under these conditions, the frequency precision is from 0.5 to 2 cm^{-1} depending on both the band intensity and the signal to noise ratio.

The equilibrium constants for imidazole or imidazolate binding to ferriprotoporphyrin were determined by spectrophotometric titrations according to methods previously described (Momenteau 1973; Yoshimura and Ozaki 1984).

The spectrophotometric measurements were done on Cary 118C or Beckman DU7 recording spectrophotometers.

Results and discussion

Absorption spectroscopy of iron(III) derivatives

The electronic absorption spectrum of Fe(III)PP$(ImH)_2$ at pH 7.5 in a 2% aqueous cetyltrimethylammonium bromide (CTABr) solution is characterized by α, β and Soret band maxima at 562.0, 536.0 and 414.0 nm, respectively (Fig. 1 A). Alkaline titration of this complex results in a gradual redshift of the absorption bands in the 8.5–12 pH range, the final compound exhibiting peak maxima at 576.0, 546.5 and 421.5 nm (Fig. 1 A). A plot of the apparent Soret maximum as a function of pH (Fig. 1 B) as well as titrations at fixed wavelengths (414.0 and 421.5 nm) (not shown) are in agreement with any of the following four reaction sequences: *i)* a sequential substitution of the two bound ImH for two hydroxide anions, *ii)* a loss of an acidic proton of one of the bound ImH with a pK_a value of 9.0, followed by a substitution of the remaining ImH for a OH^- anion, *iii)* an ImH → OH^- substitution, followed by a loss of the acidic proton of the remaining bound ImH with a pK_a value of 10.8 or *iv)* a sequential loss of the two acidic protons of the bound ImH with pK_a values of 9.0 and 10.8, according to the following sets of reactions:

$$\mathrm{FePP(ImH)_2} \underset{}{\overset{-\mathrm{ImH},+\mathrm{OH^-}}{\rightleftharpoons}} \mathrm{FePP(ImH)(OH^-)} \overset{-\mathrm{ImH},+\mathrm{OH^-}}{\rightleftharpoons} \mathrm{FePP(OH^-)_2} \quad (1)$$

$$\mathrm{FePP(ImH)_2} \overset{-\mathrm{H^+}}{\rightleftharpoons} \mathrm{FePP(ImH)(Im^-)} \overset{-\mathrm{ImH},+\mathrm{OH^-}}{\rightleftharpoons} \mathrm{FePP(Im^-)(OH^-)} \quad (2)$$

$$\mathrm{FePP(ImH)_2} \overset{-\mathrm{ImH},+\mathrm{OH^-}}{\rightleftharpoons} \mathrm{FePP(ImH)(OH^-)} \overset{-\mathrm{H^+}}{\rightleftharpoons} \mathrm{FePP(Im^-)(OH^-)} \quad (3)$$

$$\mathrm{FePP(ImH)_2} \overset{-\mathrm{H^+}}{\rightleftharpoons} \mathrm{FePP(ImH)(Im^-)} \overset{-\mathrm{H^+}}{\rightleftharpoons} \mathrm{FePP(Im^-)_2} \quad (4)$$

On the other hand, the spectrum of Fe(III)PP$(ImH)_2$ in a 2% aqueous sodium dodecylsulphate (NaDS) has no sensitivity to pH between pH 6 and pH 11 (figure not shown).

In order to ensure that the spectral transitions observed for Fe(III)PP$(ImH)_2$ in aqueous CTABr solutions are not due to a hydroxide coordination to Fe(III)PP, the bis(1-methylimidazole) (1MeIm) and the bis(pyridine) complexes of Fe(III)PP were titrated under identical experi-

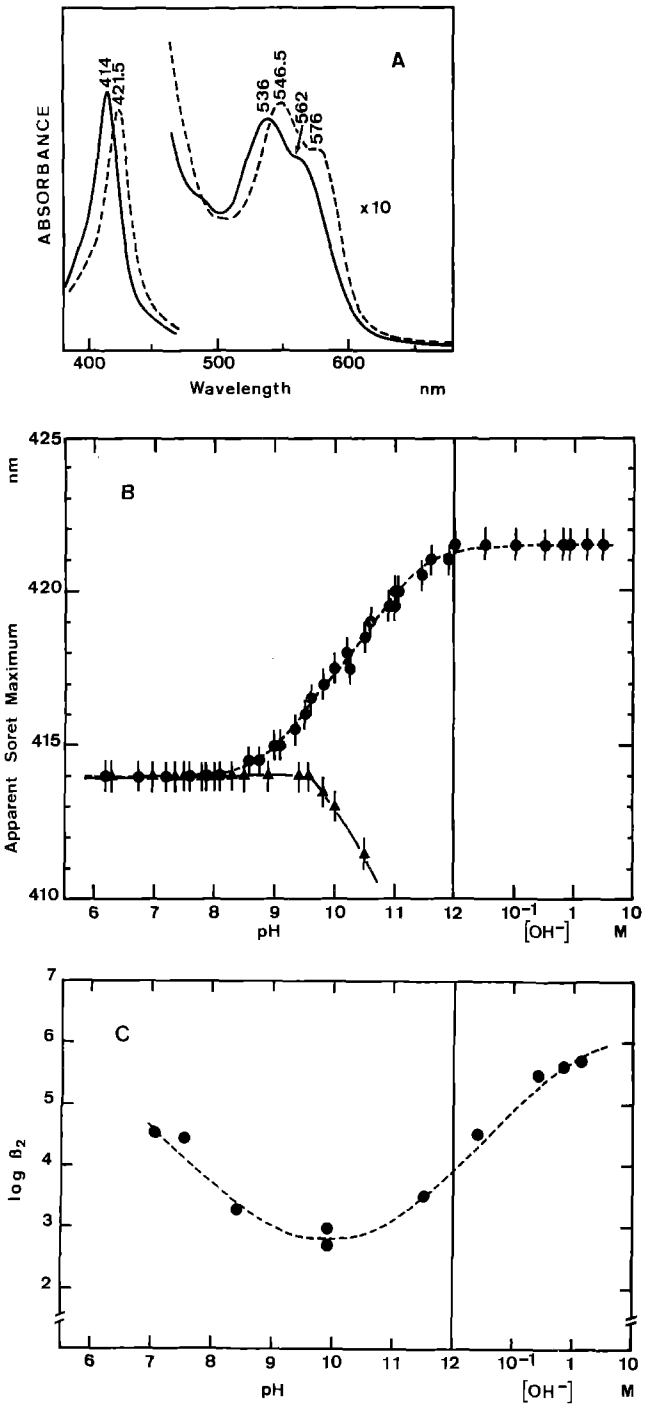

Fig. 1. **A** Electronic absorption spectra of Fe(III)PP(ImH)$_2$ (—) and of Fe(III)PP(Im$^-$)$_2$ (- - -) in 2% aqueous CTABr solutions; **B** pH- and hydroxide concentration-dependence of the Soret maximum of Fe(III)PP(ImH)$_2$ (circle) and of Fe(III)PP(1MeIm)$_2$ (triangle) in 2% aqueous CTABr solutions. Ligand concentrations: 0.85 M; the dotted curve represents a theoretical fit to the experimental points according to two Henderson-Hasselbach equations with pK_a values of 9.0 and 10.8 and implies the assumption that the Soret maxima are at 414.0, 417.0 and 421.5 nm for Fe(III)PP(ImH)$_2$, Fe(III)PP(ImH)(Im$^-$) and Fe(III)PP(Im$^-$)$_2$, respectively; **C** pH- and OH$^-$ concentration-dependence of the equilibrium formation constant (β_2) of Fe(III)PP(Im*)$_2$ in 2% aqueous CTABr solutions (see text); the dotted curve represents a theoretical fit to the experimental points according to two Henderson-Hasselbach equations with pK_a values of 9.0 and 10.8 and corresponds to values of binding constant of 1.7×10^5, 5×10^2 and 1.2×10^6 M^{-2} for Fe(III)PP(ImH)$_2$, Fe(III)PP(ImH)(Im$^-$) and Fe(III)PP(Im$^-$)$_2$, respectively

mental conditions. The Fe(III)PP(1MeIm)$_2$ complex exhibits no significant spectral sensitivity to pH between 7 and 9.5 (Fig. 1B). At pH above 9.5, the Soret band is blue-shifted, indicative of a displacement of the bound 1MeIm by OH$^-$ and of the formation of a hemin-type complex (Soret band maximum at 399 nm). A similar pattern of behaviour is observed for the bis(pyridine) complex (figure not shown). Therefore, the alkaline transitions observed in Fig. 1B for Fe(III)PP(ImH)$_2$ cannot be ascribed to the formation of a bis(hydroxide) complex of Fe(III)PP (reaction (1)).

On the other hand, we checked that all along the titration of Fe(III)PP(ImH)$_2$, two imidazole-type rings (imidazole or imidazolate) remain coordinated to the ferric heme. For this purpose, we measured spectrophotometrically the apparent association constant of imidazole to FePP(III) between pH 7 and a hydroxide concentration of 2 M. In this large range of alkalinity, we did not detect any formation of an intermediate mono(ImH) or mono(Im$^-$) complex and the equilibrium data fit an apparent one step-binding of two nitrogenous ligands according to:

$$\text{Fe(III)PP} + 2\ \text{Im}^* \rightleftharpoons \text{Fe(III)PP(Im}^*)_2\,, \qquad (5)$$

with the overall formation constant β_2 equal to:

$$\beta_2 = [\text{Fe(III)PP(Im}^*)_2]/([\text{Fe(III)PP}]\,[\text{Im}^*]^2) \qquad (6)$$

Im* representing either ImH or Im$^-$. The value of β_2 is, however, pH-sensitive (Fig. 1C). Indeed, taking into account the total free Im* concentration ([Im*]=[ImH]+[Im$^-$]) and the pK_a values obtained in Fig. 1B, β_2 calculated to be 1.7×10^5, 5×10^2 and 1.2×10^6 M^{-2} for Fe(III)PP(ImH)$_2$, Fe(III)PP(ImH)(Im$^-$) and Fe(III)PP(Im$^-$)$_2$, respectively (Fig. 1C). The low value obtained for the association constant of Fe(III)PP(ImH)(Im$^-$) probably indicates a destabilization of the hexacoordinated complex when the axial ligands are in different ionization states.

We therefore can safely attribute the change in visible spectra accompanying the alkaline titration of Fe(III)PP(ImH)$_2$ in aqueous CTABr solution to a sequential deprotonation of the two bound imidazoles, with pK_a values of 9.0 and 10.8 (reaction (4)). As expected, the maxima of the visible absorption bands of the (ImH)(Im$^-$) and bis(Im$^-$) complexes of ferriporphyrins are redshifted relative to those of the corresponding imidazole complexes (Mohr et al. 1967; Davies 1973; Peisach and Mims 1977; Nappa et al. 1977; Quinn et al. 1982). Moreover, the spectral data of Fig. 1B allow an estimation of the Soret band maximum of Fe(III)PP(ImH)(Im$^-$) at 417.0 ± 0.5 nm, i.e. at a wavelength ≈3 nm longer than that of Fe(III)PP(ImH)$_2$. A similar small difference (2 nm) has been reported between the Soret peak positions of bis(ImH) and (ImH)(Im$^-$) complexes of Fe(III)-tetraphenylporphyrin in dry solvents (Nappa et al. 1977; Quinn et al. 1982).

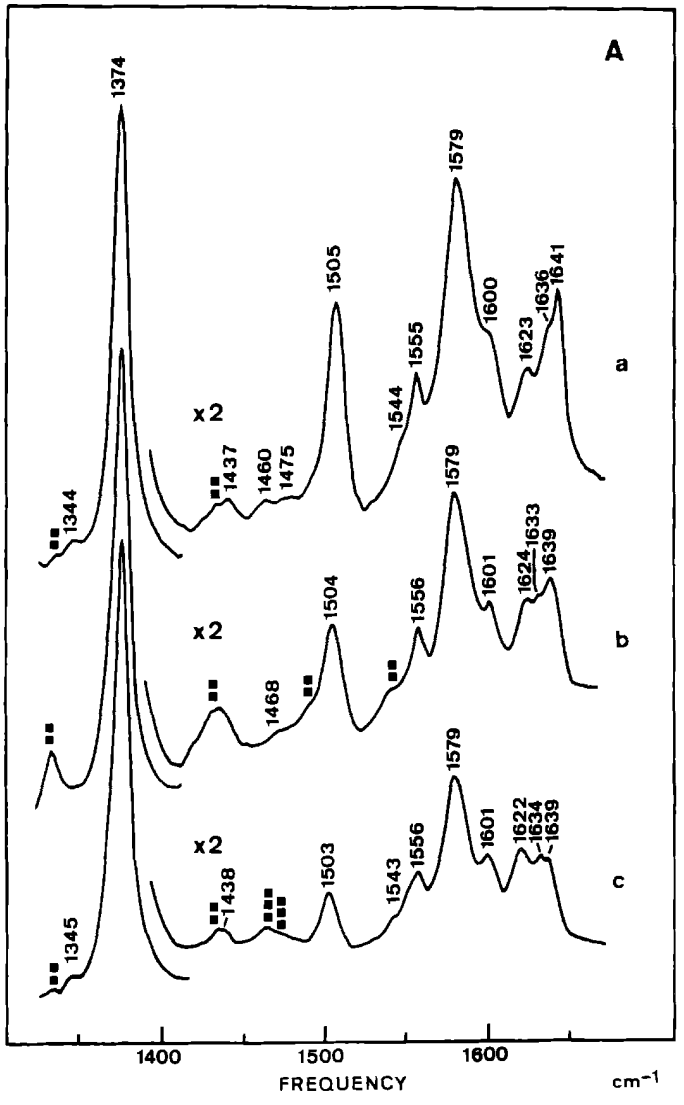

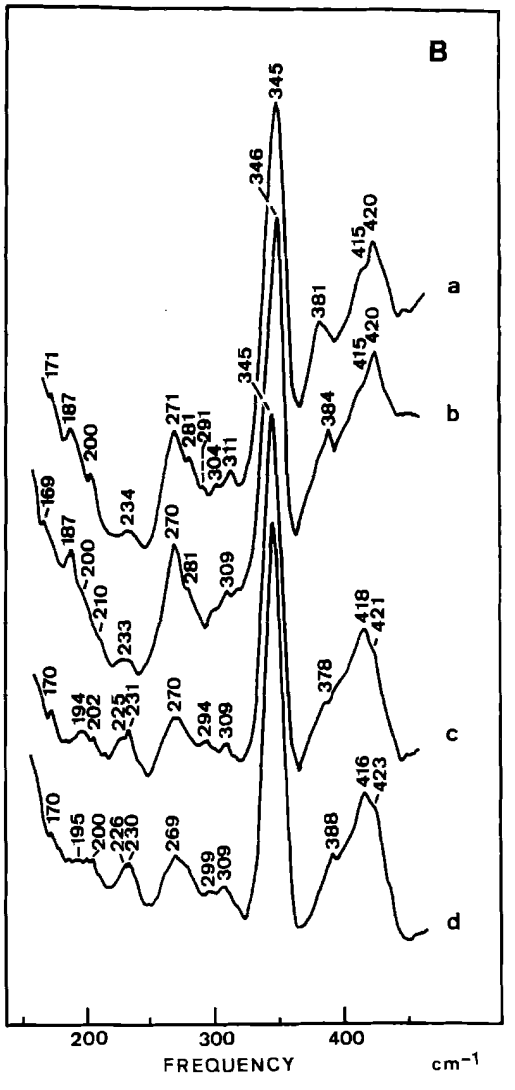

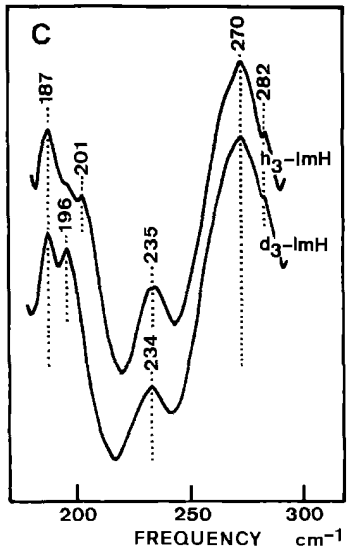

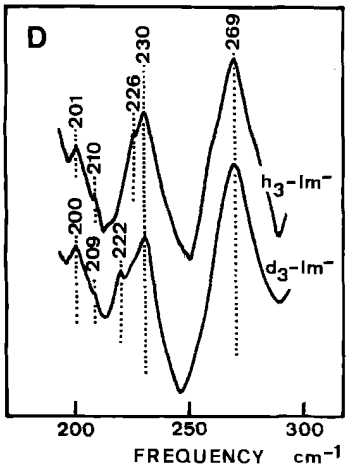

Fig. 2. **A** High frequency regions (1 300–1 650 cm^{-1}) of resonance Raman spectra of Fe(III)PP$(ImH)_2$ in 2% aqueous CTABr solutions at pH 7.5 (a), 10.0 (b) and 12.0 (c). Excitation wavelength: 441.6 nm; imidazole concentration: 0.2 M (a), 0.6 M (b) and 0.18 M (c); summation of 4–6 scans; bands marked with two and three squares correspond to free imidazole and imidazolate bands, respectively; resolution: 8 cm^{-1}; scanning speed: 25 $cm^{-1} \cdot mn^{-1}$; time constant: 5 s. **B** pH-dependence of the low frequency regions (160–450 cm^{-1}) of RR spectra of Fe(III)PP$(ImH)_2$ in 2% aqueous CTABr solutions. Excitation: 441.6 nm; imidazole concentration: 0.9 M; spectrum a: pH = 7.0; spectrum b: pH = 8.3; spectrum c: pH = 11.3; spectrum d: $[OH^-] = 2.5$ M; summation of 4–6 scans. **C** Effect of ligand perdeuterations on the 170–300 cm^{-1} regions of RR spectra of Fe(III)PP$(ImH)_2$ in 2% aqueous (H_2O or D_2O) CTABr solutions. Excitation: 441.6 nm; summations of 20 scans; imidazole (h_3-ImH or d_3-ImD) concentration: 0.2 M; pH was adjusted to 7.5 using aqueous HCl or DCl. **D** Effect of ligand perdeuterations on the 190–300 cm^{-1} regions of RR spectra of Fe(III)PP$(Im^-)_2$ in 2% aqueous (H_2O or D_2O) solutions. Excitation: 441.6 nm; summations of 20 scans; imidazole (h_3-ImH or d_3-ImD) concentration: 0.18 M; final hydroxide concentrations were adjusted at 0.1 M by addition of aqueous NaOH or NaOD

Resonance Raman spectroscopy of bis(imidazole) and bis(imidazolate) complexes of iron(III)-protoporphyrin

The high frequency resonance Raman (RR) spectra (1 300–1 650 cm^{-1}) of Fe(III)PP(ImH)$_2$ in various CTABr aqueous solutions at different pH values are presented in Fig. 2A. Considerable changes in the relative intensities of skeletal porphyrin modes are observed when the pH is increased. All the observed frequencies are in agreement with the expected low-spin character of bis(ImH), mono(ImH)-mono(Im^-) and bis(Im^-) complexes of Fe(III)PP and are not significantly affected by the axial ligand ionizations.

The low frequency regions (150–450 cm^{-1}) of RR spectra (Fig. 2B) exhibit more significant frequency variations with pH, especially in the 180–250 cm^{-1} region where modes involving stretching of axial bonds are observed or expected (Desbois and Lutz 1981, 1983; Mitchell et al. 1987). Axial ligand perdeuteration (h_3-ImH → d_3-ImD) on Fe(III)PP(ImH)$_2$ produces a 5± 1 cm^{-1} downshift of a weak 201 cm^{-1} band (Fig. 2C). This isotopic sensitivity is in accord with the previous assignment of this band to a symmetric Fe-[N(ImH)]$_2$ stretching mode (Desbois and Lutz 1983; Choi and Spiro 1983) (Table 1). In the case of the Fe(III)PP(Im^-)$_2$ complex, ligand perdeuteration (h_3-Im^- → d_3-Im^-) shifts a specific 226 cm^{-1} band by 4±1 cm^{-1} (Fig. 2D, Table 1). This line is therefore assignable to the symmetric Fe-[N(Im^-)]$_2$ stretching mode. Indeed, a triatom calculation with full masses of 67 and 70 a.m.u. for h_3-Im^- and d_3-Im^-, respectively, gives a theoretical shift of 4.9 cm^{-1}.

Fe(III)PP(ImH)$_2$ in aqueous solutions without dispersing agent (detergent or solvent) exhibits an absorption spectrum characteristic of π-aggregation (Gallagher and Elliott 1973). The frequency of the Fe-[N(ImH)]$_2$ stretching mode of aqueous Fe(III)PP(ImH)$_2$ which has been characterized at 200±1 cm^{-1} (Desbois and Lutz 1983; Choi and Spiro 1983; Mitchell et al. 1987) is not significantly affected by a pH increase from 7.5 to 11.3 (figure not shown). This demonstrates that the axial ligands of aggregated Fe(III)PP(ImH)$_2$ cannot be ionized in this pH range. This conclusion is the same as that we can draw from the insensitivity to pH of the absorption spectrum of Fe(III)PP(ImH)$_2$ in aqueous NaDS solution (see above). Therefore, the deprotonation effects observed when Fe(III)PP(ImH)$_2$ is dissolved in aqueous CTABr solution appear to be linked to specific interactions between the Fe(III)PP(ImH)$_2$ complexes and the micelles of cationic detergent (vide infra).

Table 1. Frequencies (cm^{-1}) of ν_s (Fe-L_2) and axial force constants (mdyne/Å) for various bis(imidazole) and bis(imidazolate) complexes of Fe(III)- and Fe(II)-PP

Compound	ν_s (Fe-L_2)	K (Fe-L)[b]
Fe(III)PP(ImH)$_2$		
aggregated	200 (195)[a]	1.60
aqueous CTABr	201 (196)[a]	1.62
Fe(III)PP(Im^-)$_2$		
aqueous CTABr	226 (222)[a]	2.02
Fe(II)PP(ImH)$_2$		
aggregated "neutral pH form"	203 (199)[a]	1.65
"high pH form"	200 (196)[a]	1.60
aqueous CTABr	203 (198)[a]	1.65
Fe(II)PP(Im^-)$_2$		
aqueous CTABr	212 (207)[a]	1.77

[a] Observed frequency with perdeuterated ligands

[b] Calculated force constants assuming a linear harmonic L-Fe-L oscillator with full masses for the axial ligands, i.e. 68 and 67 a.m.u. for h_3-ImH and h_3-Im^-, respectively

Absorption spectroscopy of iron(II)-protoporphyrin derivatives

The electronic absorption spectrum of Fe(II)PP(ImH)$_2$ in aqueous CTABr solutions shows visible bands at 560.5, 530.5 and 426.5 nm (Fig. 3A) and presents no pH-sensitivity between pH 6 and 12. However, titrations at high alkaline concentrations (higher than 0.1 M) reveal red-shifts of α, β and Soret bands (Fig. 3A, B). Unfortunately, the spectral characteristics of the final product cannot be directly obtained because of a detergent precipitation at hydroxide concentration higher than 2.6 M. Titrations at fixed wavelengths (426.5 and 433.0 nm) as well as a plot of the apparent Soret maximum as a function of the hydroxide concentration, however, allow the observation of two spectral transitions (Fig. 3B). The titrations at fixed wavelengths characterize these two transitions with half effects at OH^- concentrations of 0.1 and 1.26 M (Fig. 3B, inset). On the other hand, a plot of apparent Soret maximum versus hydroxide concentration (Fig. 3B) fits with a Soret peak at 428.0±0.5 nm and 436.0±0.5 nm for the intermediate and final product of the alkaline titration of Fe(II)PP(ImH)$_2$, respectively. These band positions could be attributed to a formation of mono(ImH) and mono(Im^-) high spin complexes of Fe(II)PP. However, the mono(2-methylimidazole) and mono(2-methylimidazolate) complexes of Fe(II)PP which are easily prepared in 2% aqueous CTABr solutions exhibit Soret band maxima at higher wavelength (432.0 and 441.5 nm, respectively), with much lower extinction coefficients (Desbois A, unpublished results). Additionally, the absorption spectrum of Fe(II)PP(1MeIm)$_2$ in CTABr aqueous solution do not present any sensitivity to hydroxide addition (Fig. 3B). We can therefore attribute the spectral changes observed in the alkaline titrations of Fe(II)PP(ImH)$_2$ in aqueous CTABr solutions to the deprotonation of the two bound imidazoles with calculated pK_a values of 13.0 and 14.1 (Yagil 1967b). As in the case of the ferric compound, the use of NaDS in place of CTABr as a detergent apparently prevents the imidazole deprotonations in Fe(II)PP(ImH)$_2$ (data not shown).

Detergent effects and heme-micelle interactions

Our spectrophotometric investigations showed that the Fe(II)- and Fe(III)PP(Im^-)$_2$ compounds are formed in the presence of CTABr, a cationic detergent, but not in the

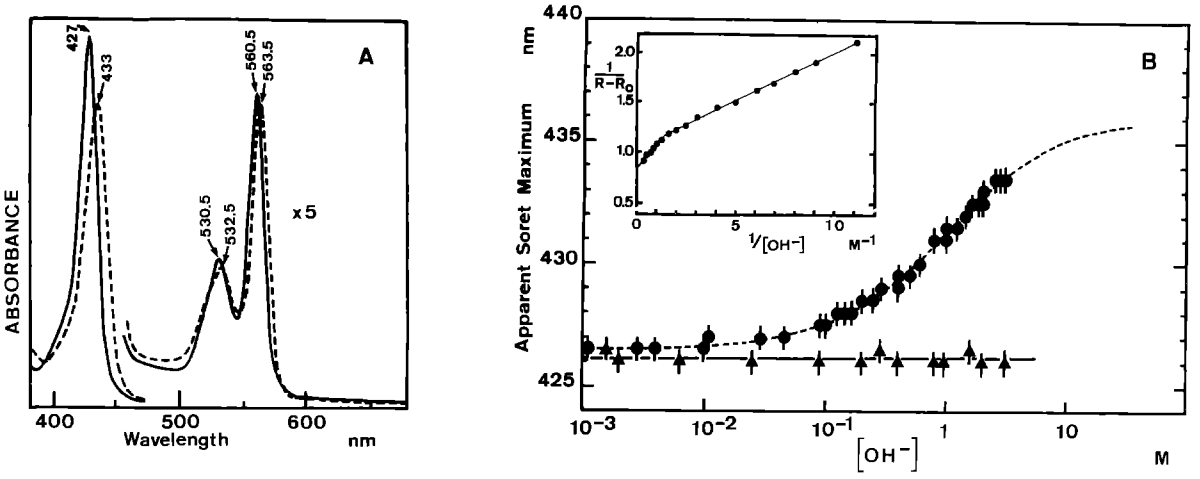

Fig. 3. **A** Electronic absorption spectra of Fe(II)PP(ImH)$_2$ (—) and of a mixture of Fe(II)PP(ImH)(Im$^-$) with Fe(II)PP(Im$^-$)$_2$ (- - -) in 2% aqueous solutions; **B** hydroxide concentration-dependence of the Soret maximum of Fe(II)PP(ImH)$_2$ (circle) and of Fe(II)PP(1MeIm)$_2$ (triangle) in 2% aqueous CTABr solutions. Ligand concentration: 0.9 M; the theoretical curve is drawn according to a two-step ionization of Fe(II)PP(ImH)$_2$ with pK$_a$ values of 13.0 and 14.1 (see text). *Inset*: plot of $1/(R-R_0)$ versus 1/[OH$^-$]; R represents the ratio of optical densities at 427 and 433 nm, observed at a known hydroxide concentration, R_0 being the R value obtained at pH 7

presence of NaDS, an anionic one. This observation reveals the strong influence of polar head groups in the deprotonation of axial ligands. Although a matter of controversy, the most simplified pictures of micellar structures divide the micelle into three regions: a lipophilic core containing the surfactant tails, the Stern layer containing the head groups and a large fraction of the counterions and, finally, the Gouy-Chapman layer which extends radially out into the aqueous phase and which contains the remaining counterions (Menger and Doll 1984; Paleos 1985). Considerable experimental evidence indicates that charged or polar molecules reside at the Stern layer (Menger and Doll 1984; Paleos 1985). Taking into account the polar character of the two bound ImH as well the ionic character of the two propionate heme groups, one may assume that FePP(ImH)$_2$ is located in this micellar region. In this case, the counterion Br$^-$ of CTABr should be easily displaced by OH$^-$ during the alkaline titrations. This should facilitate the ionization of bound ImH. In the NaDS micelles, the counterions in close vicinity with heme complexes would be Na$^+$. In this situation, the OH$^-$ ions could not be located in the Stern layer and hence could not interact with the heme ligands. Therefore, the present experimental observations are in accordance with a heme located in the Stern layer of detergent micelles.

Moreover, the two-step deprotonations of Fe(II)- and Fe(III)-PP(ImH)$_2$ indicate a difference in solvent accessibility of axial ligands or/and an electronic effect associated with the basicity of the trans ligand. In the former hypothesis, the differences in the pK$_a$ values may suggest that the two heme faces are in different environments and have different solvent accessibilities, excluding a radial inclusion of heme complexes into the micelles (Simplicio 1972). An interfacial position of these complexes with one ImH ligand pointing toward the hydrophobic micelle core and the other toward the aqueous phase could easily explain a sequential deprotonation of axial ligands. Moreover, the imidazolate ligand pointing toward the external part of the CTABr micelle could be stabilized by an ionic interaction with a positively charged trimethylammonium head group. A similar interfacial location has been proposed for chlorophyll *a* in reverse micelles (Brochette et al. 1987). Alternatively, the two-step deprotonations of the axial ligands of Fe(II)- and Fe(III)-PP(ImH)$_2$ may reflect a trans effect, the deprotonation of one imidazole increasing the proton affinity of its trans ligand. This effect could be generated by the increase in the negative charge on the porphyrin complex upon imidazolate formation.

We have also to take into account that free ImH and Im$^-$ could be present in the Stern layer. In particular, ImH is both a H-bonding donor and acceptor. Therefore, the Fe-ligand stretching modes observed in the present study could be affected by H-bonding interactions between bound and free ligands.

Resonance Raman spectroscopy of bis(imidazole) and bis(imidazolate) complexes of iron(II)-protoporphyrin

In order to differentiate the frequencies of skeletal porphyrin modes arising from the Fe(II)PP(ImH)$_2$, Fe(II)PP(ImH)(Im$^-$) and Fe(II)PP(Im$^-$)$_2$ species, we used three different excitations, at 413.1, 441.6 and 457.9 nm, each insuring optimal resonance at the Soret bands of each of these species (Soret maximum at 426.5, 428 and 436 nm), respectively. Two steps of the alkaline titration of Fe(II)PP(ImH)$_2$, excited at 413.1 nm, are presented in Fig. 4. These spectra show that the apparent frequencies of skeletal modes ν_4 (1 360 → 1 358 cm^{-1}), ν_{11} (1 533 → 1 526 → 1 517 cm^{-1}), ν_{38} (1 556 → 1 554 cm^{-1}) and ν_{10} (1 616 → 1 613 cm^{-1}) are significantly downshifted upon ionization of one or both of the coordinated imidazoles. The ν_{11} mode appears to be the most sensitive to axial deprotonation. In particular, 413.1 nm-excitation of Fe(II)PP(ImH)$_2$ in 0.25 M NaOH permits us to assign a 1 526 cm^{-1} band to the ν_{11} mode of

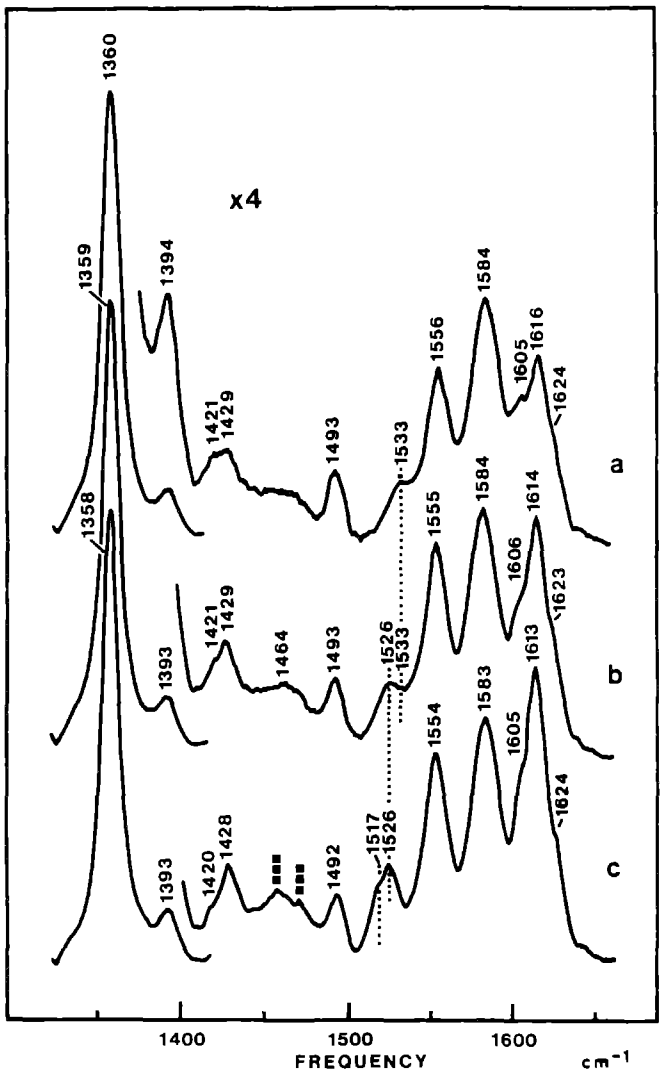

Fig. 4. High frequency regions (1 300–1 650 cm^{-1}) of RR spectra of Fe(II)PP(ImH)$_2$ in 2% aqueous CTABr solutions at pH 7.5 (a), in 0.25 M NaOH (b) and in 2.25 M NaOH (c). Excitation: 413.1 nm; summations of 4–5 scans; imidazole concentration: 0.9 M; bands marked with three squares arise from free imidazolate

Fe(II)PP(ImH)(Im$^-$) (Fig. 4, spectrum b). At higher hydroxide concentrations (2.0–2.5 M), the ν_{11} mode of Fe(II)PP(Im$^-$)$_2$ appears as a shoulder of variable intensity at 1 517 cm^{-1} on the band at 1 526 cm^{-1} (ν_{11} of Fe(II)PP(ImH)(Im$^-$)) (Fig. 4, spectrum c).

In the low frequency regions of RR spectra of Fe(II)PP(ImH)$_2$ in aqueous NaDS solutions, a 203 cm^{-1} band has been previously assigned to the symmetric stretching mode of axial ligands with the iron atom [ν_s (Fe-(ImH)$_2$] (Desbois and Lutz 1981). This band is found again in the spectrum of Fe(II)PP(ImH)$_2$ in aqueous CTABr solutions excited at 441.6 nm (Fig. 5A, B). The alkaline titration of this compound permits the observation of new Raman bands in the 200–230 cm^{-1} regions (Fig. 5A, B). At moderate hydroxide concentrations (ca. 0.1 M), a 207 cm^{-1} line is associated with the Fe(II)PP(ImH)(Im$^-$) complex (Fig. 5B). At higher alkaline concentrations, this band decreases in intensity and a new one rises at 212 cm^{-1} (Fig. 5B). We assign it to the Fe(II)PP(Im$^-$)$_2$ complex. Also present in these spectra, as a minor contribution, are lines at $\approx$223 and 230 cm^{-1} (Fig. 5A, B). Control experiments, using low imidazole concentrations (0.01–0.1 M), however show that these latter two bands correspond to the pentacoordinated complexes, Fe(II)PP(ImH) and Fe(II)PP(Im$^-$) (Desbois A, unpublished data). Furthermore, we previously characterized a specific 223 cm^{-1} band for Fe(II)PP(ImH) in NaDS aqueous solution (Desbois and Lutz 1981). Therefore, the bis(base) complexes of Fe(II)PP appear to be slightly destabilized by high hydroxide concentrations and, likely, by high ionic strengths.

Perdeuterations of axial ligands of Fe(II)PP(ImH)$_2$, Fe(II)PP(ImH)(Im$^-$) and of Fe(II)PP(Im$^-$)$_2$ in CTABr aqueous solutions induce the 203, 207 and 212 cm^{-1} bands to shift by 4 ± 1, 4 ± 1 cm^{-1} and 5 ± 1 cm^{-1}, respectively (Fig. 6A–C). On the basis of this isotopic sensitivity, we can assign these three bands to modes involving the symmetric stretching of axial ligands (Table 1).

In the absence of dispersing agents, Fe(II)PP(ImH)$_2$ forms aggregates in which the chromophore structure and environment have not yet been well characterized. Optical absorption spectra of these aggregates exhibit double Soret bands which are most likely due to exciton interactions between neighbouring metalloporphyrins (Mitchell et al. 1987; Selensky et al. 1981). This splitting as well as the B- and Q-band intensities are pH- and ionic strength-dependent, as well as porphyrin- and ligand-concentration-dependent. Figure 7 illustrates a pH effect on the absorption spectrum of aqueous Fe(II)PP(ImH)$_2$ consisting in both a redshift of visible bands and a strong intensity loss of the Soret transition.

The RR spectra of aggregated Fe(II)PP(ImH)$_2$ in various solution conditions have been investigated and indicate the existence of two spectroscopically distinguishable forms (Fig. 8). Using moderate (0.1–0.2 M) or high (1 M) ImH concentrations, in the 7–8 pH range, a "neutral pH form" predominates. The RR frequencies of the skeletal porphyrin modes as well as the Fe-(ImH)$_2$ stretching frequency are not significantly different from those of Fe(II)PP(ImH)$_2$ in aqueous detergent solutions, the spectral differences concerning changes in the relative band intensity.

On the other hand, a "high pH form" of π-π complexes of Fe(II)PP(ImH)$_2$ is essentially observed in the 10–12 pH range, using lower imidazole concentrations (0.10–0.15 M), and in the 8–12 pH range, using a higher imidazole concentration (1 M). In the higher frequency regions of RR spectra, modes ν_{11}, ν_{38}, ν_{37} and ν_{10}, observed at 1 535, 1 555, 1 601 and 1 619 cm^{-1} for the "neutral pH form", are upshifted at 1 539, 1 560, 1 604 and 1 616 cm^{-1} for the "high pH form", respectively (Fig. 8A). In the lower frequency regions, a 3 cm^{-1} downshift of the Fe-(ImH)$_2$ stretching mode is detected. It occurs from 203 cm^{-1} for the "neutral pH form" to 200 cm^{-1} for the "high pH" one (Fig. 8B). Both these bands exhibit a 4.5 ± 0.5 cm^{-1} downshift upon h_3-ImH $\rightarrow$ d_3-ImD substitution (data not shown). These identical isotopic shifts show that the 203 $\rightarrow$ 200 cm^{-1} displacement of the ν [Fe-(ImH)$_2$] mode is related to a slight pH effect on the axial ligands and not to a different accidental mixing of the axial symmetric mode with a porphyrin mode.

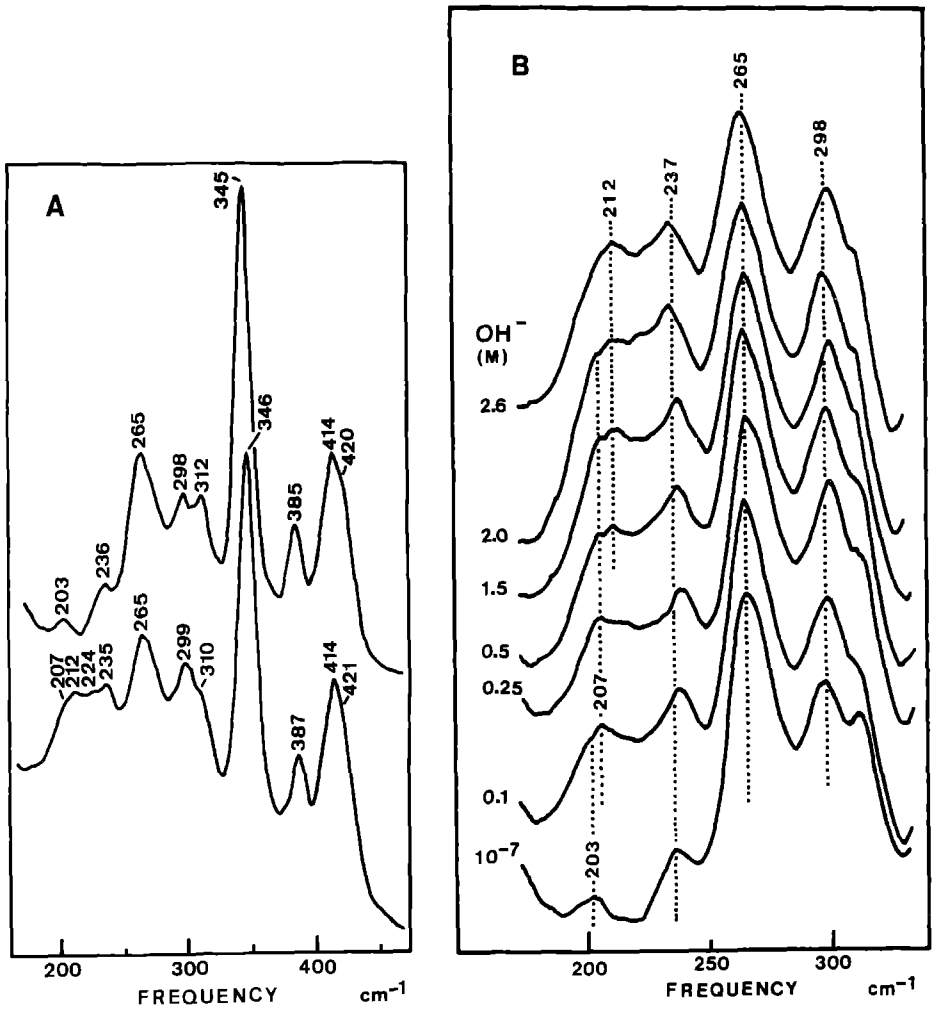

Fig. 5 A, B. Low frequency regions of RR spectra of Fe(II)PP(ImH)$_2$ and of a mixture of Fe(II)PP(ImH)(Im$^-$) with Fe(II)PP(Im$^-$)$_2$ in 2% aqueous CTABr solutions. **A** Low frequency regions (150–450 cm^{-1}) of Fe(II)PP(ImH)$_2$ at pH 7.5 and in 2.1 M NaOH. Excitation: 441.6 nm; imidazole concentration: 0.9 M; summation of 6 scans. **B** Hydroxide concentration-dependence of the 180–320 cm^{-1} regions of RR spectra of Fe(II)PP(ImH)$_2$. Excitation: 441.6 nm; imidazole concentration: 0.9 M

These spectral modifications probably reflect the existence of two types of porphyrin aggregates, the equilibrium between these two forms depending on the pH and ionic strength of the solution. In particular, a slight modification in the H-bonding interactions of axial ligands (vide supra) could explain the differences observed in the RR spectra.

The spectral descriptions made in this section show that the structures of the heme and its axial bonds are sensitive to the solvent conditions and composition. In the two following sections, we shall discuss more specifically these structures deduced from the present Raman study.

Stretching modes of axial bonds

The symmetric Fe-[N(ImH)$_2$] stretching mode of Fe(II)- and Fe(III)-PP(ImH)$_2$ has been assigned to a band located at 199–203 cm^{-1} (Desbois and Lutz 1981, 1983; Choi and Spiro 1983; Mitchell et al. 1987). The RR data presented here for the same compounds in CTABr aqueous solutions or in water are consistent with these earlier conclusions.

We have now identified and characterized the symmetric Fe-[N(Im$^-$)]$_2$ stretching mode of Fe(II)- and Fe(III)-PP(Im$^-$)$_2$ in aqueous CTABr solutions at 212 and 226 cm^{-1}, respectively. Compared to the 199–203 cm^{-1} frequency range of bis(imidazole) complexes, these frequencies show that the imidazole deprotonations of FePP(ImH)$_2$ induce a strengthening of the axial bonds. Theoretical considerations indicate that Im$^-$ has a stronger σ electron donor capability than ImH (Demoulin and Pullman 1978). For the first time, this electronic effect is experimentally demonstrated for the bis(imidazole) and bis(imidazolate) complexes of Fe(II)- and Fe(III)-PP. Moreover, while the oxidation state of the iron atom has no significant influence on the stretching mode of the Fe-N(ImH) bonds of FePP(ImH)$_2$, oxidation of the iron of the FePP(Im$^-$)$_2$ complexes induces a 14 cm^{-1} upshift of this mode (Table 1). Both a higher σ bonding capability of Fe(III) over Fe(II) and a higher equatorial back-bonding of the metal ion in Fe(II)PP(Im$^-$)$_2$ than in Fe(II)PP(ImH)$_2$ could explain this substantial frequency shift (vide infra).

Using a triatomic linear model and the present stretching frequencies, axial bond strengths of 1.62 and 2.02 mdyne/Å are calculated for the Fe(III)-N(ImH) and Fe(III)-N(Im$^-$) bonds, respectively (Table 1). Considering a Fe-N(ImH) bond length of 1.96–1.99 Å for Fe(III)PP(ImH)$_2$ (Collins et al. 1972; Scheidt et al. 1987) and using Badger's rule (Herschbach and Laurie 1961), the present Raman data indicate that the axial bond lengths are shortened by 0.08 Å when the imidazoles are deprotonated. Up to now, a single crystal structure of a

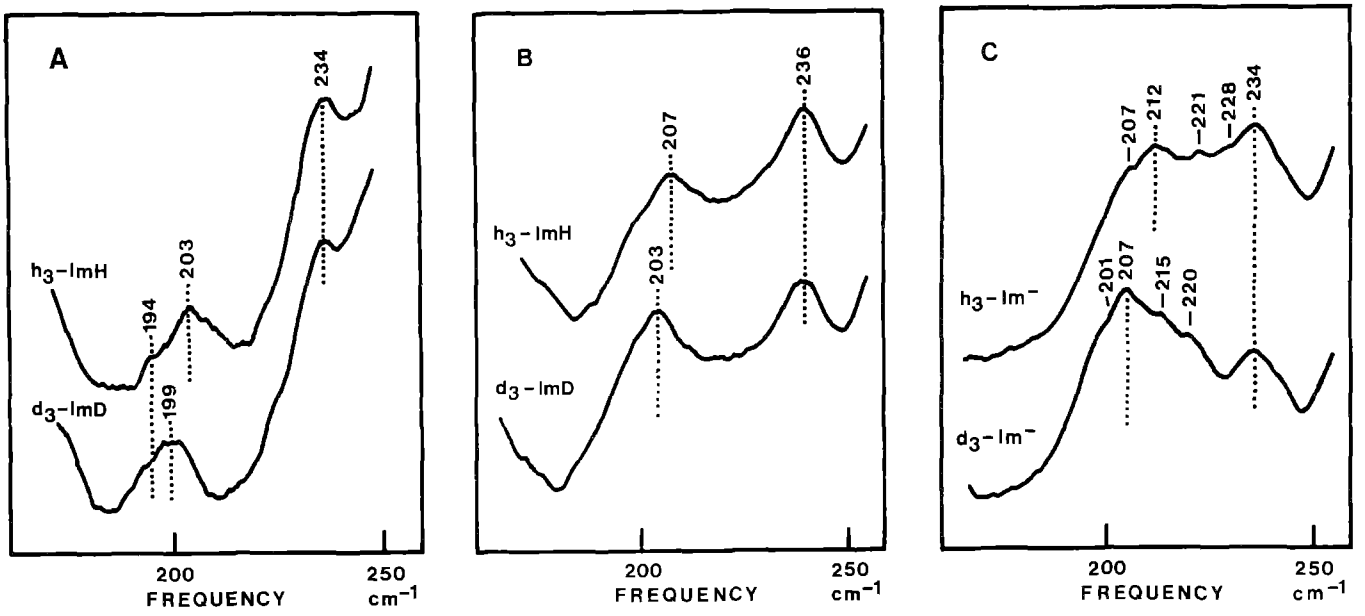

Fig. 6A–C. Determination of the symmetric stretching mode of axial ligands with the iron atom of Fe(II)PP(ImH)$_2$, Fe(II)PP(ImH)(Im$^-$) and of Fe(II)PP(Im$^-$)$_2$. **A** Effects of ligand perdeuterations on the 150–250 cm^{-1} regions of RR spectra of Fe(II)PP(ImH)$_2$ in 2% aqueous CTABr solutions; pH were adjusted at 8.0 using HCl (or DCl) in H_2O (or D_2O); **B** effects of ligand perdeuterations on the 150–250 cm^{-1} regions of RR spectra of Fe(II)PP(ImH)(Im$^-$) with Fe(II)PP(ImH)$_2$ in 2% aqueous CTABr solutions; the final hydroxide concentrations were adjusted at 0.12 M using NaOH (or NaOD) in H_2O (or D_2O); **C** effects of ligand perdeuterations on the 150–250 cm^{-1} regions of RR spectra of Fe(II)PP(Im$^-$)$_2$ with Fe(II)PP(ImH)(Im$^-$) in 2% aqueous CTABr solutions; the final hydroxide concentrations were adjusted at 2.3 M using NaOH (or NaOD) in H_2O (or D_2O). Excitation: 441.6 nm; each spectrum is the summation of 20 scans

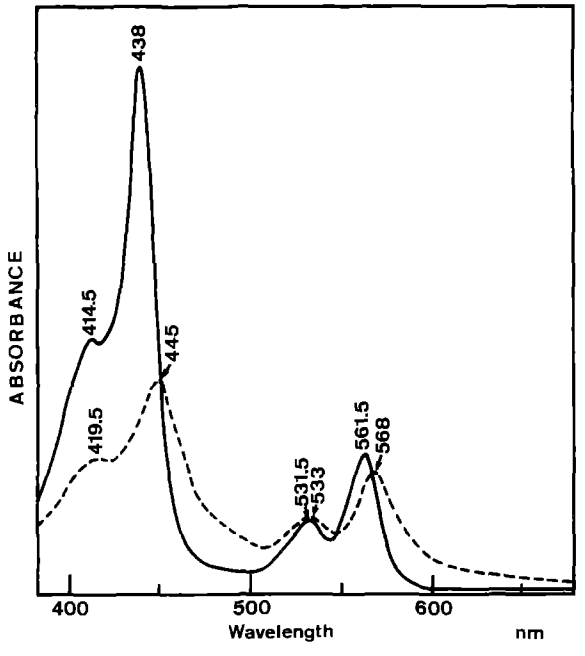

Fig. 7. Electronic absorption spectra of aggregates of Fe(II)PP(ImH)$_2$ in water at pH 7.5 (—) and 12.3 (- - -). Experimental conditions: aggregations were induced by the use of high porphyrin concentrations (0.8 mg · ml^{-1}) and moderate imidazole concentrations (0.125 M); the optical absorption spectra were measured using 0.1 mm path length cuvettes; pH were adjusted using aqueous HCl or NaOH

parent complex, namely that of the bis(4-methylimidazolate) complex of Fe(III)-tetraphenylporphyrin has been solved (Quinn et al. 1983). For a similar imidazole ring orientation relative to the Fe-N (pyrrole) bonds, the axial bond length is shortened by 0.060 Å upon N_1-H deprotonation. Our Raman data indicate that the upper limit of the bond shortening (0.072 Å) allowed by the 0.012 Å standard error of this X-ray study is most probably to be retained.

No crystallographic data are available for any bis(imidazolate) complex of a ferroporphyrin. However, the symmetric stretching mode of the axial bonds has been assigned at 203 and 212 cm^{-1} for Fe(II)PP(ImH)$_2$ and Fe(II)PP(Im$^-$)$_2$, respectively. These frequencies correspond to force constants of 1.65 and 1.76 mdyne/Å for the Fe(II)-N(ImH) and the Fe(II)-N(Im$^-$) bonds, respectively, using the above linear triatomic oscillator (Table 1). Assuming a Fe(II)-N(ImH) bond length of 2.00–2.02 Å in Fe(II)PP(ImH)$_2$ (Scheidt and Gouterman 1983), deprotonation of the axial ligands is calculated to shorten the axial bond lengths by 0.025 Å, on the basis of Badger's rule (Herschbach and Laurie 1961).

A 207 cm^{-1} band is associated with the Fe(II)-(ImH)(Im$^-$) complex (Fig. 5B). Its sensitivity to ligand perdeuteration (Fig. 6B) allows us to identify it as one of the two Fe(II)-axial ligand stretching modes. Indeed, the symmetric (Raman active) and antisymmetric (IR active)

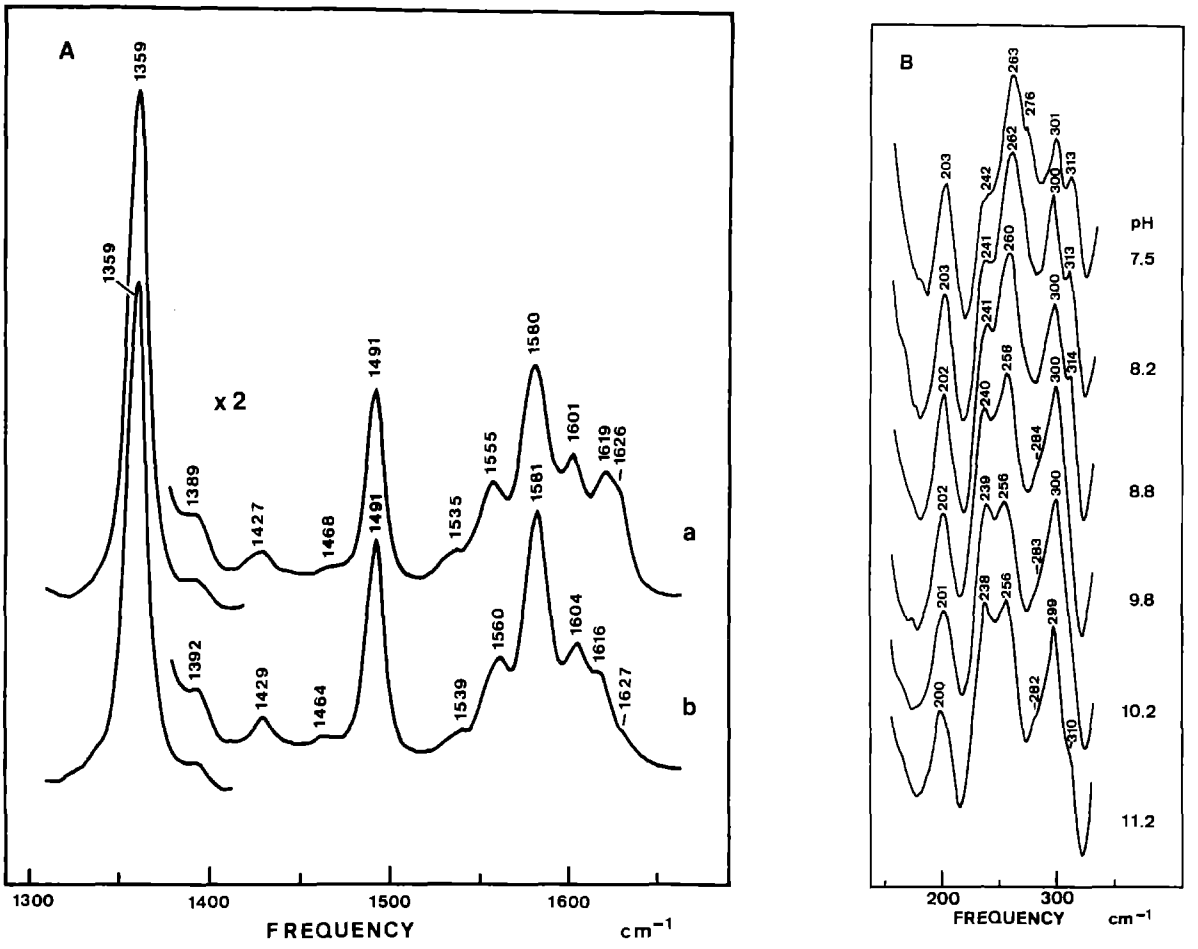

Fig. 8 A, B. RR spectra of aggregated Fe(II)PP(ImH)$_2$. **A** High frequency regions (1 300–1 650 cm^{-1}) of RR spectra of Fe(II) PP(ImH)$_2$ in water at pH 7.5 (a) and 12.3 (b). Excitation: 441.6 nm; imidazole concentration: 0.125 M. **B** pH-dependence of the low frequency regions (150–350 cm^{-1}) of RR spectra of aggregated Fe(II)PP(ImH)$_2$. Excitation: 441.6 nm; imidazole concentration: 0.125 M

stretching modes of a symmetric linear oscillator (L-Fe-L) are transformed into two strongly coupled Raman-active modes in a L-Fe-L′ asymmetric linear oscillator. In the limit that the bending force constants are much smaller than the stretching force constants, the Fe-L and Fe-L′ stretching frequencies can be determined by the following equation (Cross and Van Vlieck 1933; Wilson 1939):

$$\omega^2 = \tfrac{1}{2}(K/\mu + K'/\mu') \pm \tfrac{1}{2}\{(K/\mu + K'/\mu')^2 - (4KK'/M)\}^{1/2} \quad (7)$$

where μ, K and μ', K' are the reduced masses and force constants of the Fe-L and Fe-L′ bond, respectively. The quantity M is equal to:

$$M = (m_{Fe} \cdot m_L \cdot m_{L'})/(m_{Fe} + m_L + m_{L'}) \quad (8)$$

The frequencies (v and v') are given by: $v = \omega(2\pi c)^{-1}$ where the sign – in (7) corresponds to the predominantly Fe-L stretching mode (v), the sign + being associated with the predominantly Fe-L′ stretching vibration (v').

Setting the full masses of ImH and Im$^-$ as 68 and 67 a.m.u., respectively, and deducing the stretching force constants of Fe-ImH and Fe-Im$^-$ bonds from those obtained for the symmetric complexes (1.65 and 1.76 mdyne/Å, respectively) (Table 1), a theoretical frequency is calculated at 207 cm^{-1} for the mode predominantly involving Fe-ImH stretching. A similar calculation predicts a 5.1 cm^{-1} downshift for this mode when the ligand masses are increased by axial perdeuterations (h_3-ImH → d_3-ImD and h_3-Im$^-$ → d_3-Im$^-$). Therefore, the 207 cm^{-1} line observed for Fe(II)PP(ImH)(Im$^-$) can be assigned to a mode involving stretching of Fe-N(ImH) coupled with a Fe-N(Im$^-$) bond stretching. The mode predominantly involving Fe-N(Im$^-$) stretching is calculated at 383 cm^{-1}. It is not observed in the RR spectra.

Hence, the symmetric stretching modes of axial bonds of the bis(imidazole) and bis(imidazolate) complexes of Fe(II)- and Fe(III)-PP are observed using a 441.6 nm-excitation. This Raman activity appears neither very sensitive to the oxidation state of the iron atom nor to the ionization state of the axial ligands and will be particularly useful in the monitoring of the ν_s (His-Fe-His) mode of *b*-type cytochromes.

Porphyrin modes

The axial deprotonation of Fe(III)PP(ImH)$_2$ has no detectable influence on the frequencies of skeletal porphyrin modes (Fig. 2A). On the contrary, the frequencies of the ν_4, ν_{10}, ν_{11} and ν_{38} modes present significant sensitivity to the ionization of Fe(II)PP(ImH)$_2$ (Fig. 4). Since ν_3

(1 493–1 492 cm^{-1}) is nearly insensitive to the imidazole deprotonations (Fig. 4), these frequency shifts cannot be attributed to a marked change in the porphyrin core size (Parthasarathi et al. 1987). Mode ν_{11} is the most sensitive porphyrin mode to imidazole deprotonation, being shifted from 1 534 to 1 517 cm^{-1} (Fig. 4). It is also shifted from 1 535 to 1 539 cm^{-1} upon the "neutral → high pH form" transition of aggregated Fe(II)PP(ImH)$_2$ (Fig. 8A). This mode is assigned to a $C_\beta - C_\beta$ stretching mode (Abe et al. 1978). A larger sensitivity of the ν_{11} frequency over the ν_4 frequency has been previously observed in the RR spectra of various divalent metal-porphyrin complexes (Kim et al. 1986; Ozaki et al. 1986; Boldt et al. 1988). This effect has been attributed to an equatorial back-bonding of the metal ion (Boldt et al. 1988): the lower the ν_{11} frequency, the higher the extent of back donation of electron density from the filled d_π orbitals of the ferrous ion into the empty e_g^* porphyrin orbitals. Taking into account that a strong back-bonding has been detected in Fe(II)PP(ImH)$_2$ (Choi et al. 1982; Parthasarati et al. 1987), the low frequency of the ν_{11} mode of Fe(II)PP(Im^-)$_2$ can be attributed to an increased equatorial back-bonding. Assuming that the absolute frequency of the mode ν_{11} roughly reflects the competition which has been proposed to occur between the π system of the axial ligands and that of the porphyrin for the same electrons (Spiro and Burke 1976), this frequency is expected to be directly related to the stretching frequency of axial ligands with the iron atom. Figure 9 clearly shows an inverse correlation between these frequencies and therefore supports the above predictions. Although the 207 cm^{-1} mode of Fe(II)PP(ImH)(Im^-) is theoretically not a pure symmetric stretching mode of axial ligands against the metallic ion (vide supra), this frequency also matches with its corresponding ν_{11} frequency (1 521 cm^{-1}), suggesting that the mode composition of the 207 cm^{-1} band is not so far from that of a pure, totally symmetric L-Fe-L mode. As far as the aggregated Fe(II)PP(ImH)$_2$ complexes are concerned, Fig. 9 indicates that the axial ImH ligands are less H-bonded in the "high pH form" than in the "low pH form".

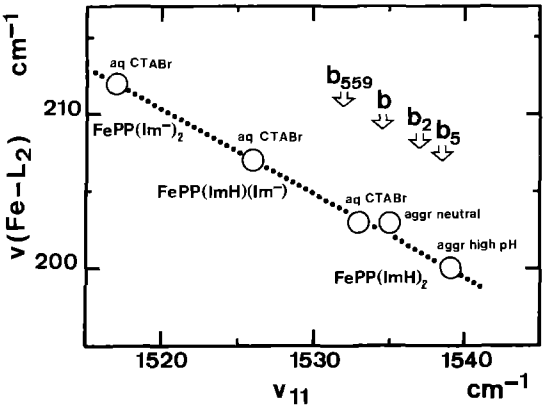

Fig. 9. Relationship between the frequency (cm^{-1}) of the symmetric stretching mode of Fe(II)PP(ImH)$_2$ in various aqueous conditions and of Fe(II)PP(Im^-)$_2$ in aqueous CTABr solutions and the corresponding frequency (cm^{-1}) of the ν_{11} porphyrin mode (see text and Table 1). The straight line is drawn according the equation: ν_s (Fe-L_2) = 1 041 − (0.5465 × ν_{11})

Therefore, the ν_{11} frequency can in principle give an estimation of axial bond strengths of reduced *b*-type cytochromes containing two histidines as heme ligands.

H-bonding at the coordinated histidylimidazoles

A hydrogen bonding interaction at a histidylimidazole may be considered as a partial deprotonation at the N_1 site. As the strength of the H bond increases, the imidazole ring acquires a more anionic character. Thus, H bonding at the axial histidylimidazoles is expected to introduce structural and electronic perturbations at the heme (ferrous or ferric) which should be intermediate between those observed for the two limiting forms, i.e. the bis(imidazole) and bis(imidazolate) complexes. Taking into account the fact that hydrogen donor strength of an ionizable grouping is directly correlated to its intrinsic acidity (Meot-Ner 1988), the pK_a values obtained for the ionizations of axial ligands of Fe(II)- and Fe(III)-PP(ImH)$_2$ indicate that the imidazole N_1-H bonds of the ferric derivative are more polarizable by 3–4 orders of magnitude than those of the ferrous derivative. Thus, H-bonding at the coordinated imidazoles exerts its effect almost totally on the ferric heme and, hence, can decrease the redox potential of the corresponding Fe(II)/Fe(III) couple by 50–100 mV (Doeff et al. 1983; Quinn et al. 1983, 1984). As suggested by Valentine et al. (1979), this differential mechanism probably constitutes an important factor in the fine tuning of oxidation-reduction potentials of cytochromes.

The present RR data indicate that the H-bonding strength of histidylimidazoles of ferric cytochromes can be evaluated from the ν_s(N(*His*)-Fe-N(*His*)) stretching frequency. As far as the ferric *b*-type cytochromes are concerned, the corresponding RR data are still scanty. For the ferrous complexes, a linear relationship is found between the frequencies of the Fe-[N(axial)]$_2$ symmetric stretching mode and the ν_{11} mode (Fig. 9). This relationship can be used to estimate the H-bonding interactions at the coordinated histidylimidazoles of reduced cytochromes from the ν_{11} porphyrin mode frequency. The frequency of the ν_{11} mode has been observed at 1 537–1 539 cm^{-1} for isolated cyt b_5 and cyt b_2 core (Adar 1975; Kitagawa et al. 1982; Desbois et al. 1989; Hobbs et al. 1990). As far as the membrane cyt *b* are concerned, ν_{11} has been observed at 1 529–1 536 cm^{-1} for diheme mitochondrial and bacterial cyt *b* (Adar and Erecinska 1974; Adar et al. 1981; Hobbs et al. 1990) and at 1 532 cm^{-1} for chloroplast cyt b_{559} (Babcock et al. 1985). The 1 529–1 536 cm^{-1} frequency may therefore reflect a stronger H-bonding at the coordinated histidylimidazoles of the transmembrane cytochromes than at those of globular cytochromes (Fig. 9).

The crystallographic structures of calf liver cyt b_5 and *Saccharomyces cerevisiae* flavocyt b_2 show similar heme-protein interactions (Mathews et al. 1972a, b; Xia and Mathews 1990). In particular, the two histidylimidazoles serving as the heme ligands have their planes nearly parallel and are each hydrogen-bonded to a carbonyl oxygen of the polypeptide backbone. The ν_{11} frequencies of cyt b_5 and cyt b_2 are relatively high, hence indicating

weak H-bonding at the coordinated *His* of these hemoproteins (Fig. 9). On the other hand, no information is yet available on the three-dimensional structure of any transmembrane cyt *b*. Nevertheless, amino-acid sequences and amphipathic profiles predict that the peptide chains of cytochromes *b* of mitochondrial $b\,c_1$ and chloroplast b_6f complexes are very homologous and arranged into several α-helices traversing the lipid bilayer (Saraste 1984; Widger et al. 1984; Cramer et al. 1987; Hauska et al. 1988). In these models, the two hemes crosslink two of these helices via four *His* ligands. An inspection of amino acid sequences does not permit us to locate any putative proton acceptor residue that could interact with any of these *His* ligands. However, one may note the systematic presence of a basic residue (*Arg*, *His* or *Lys*) 3 or 5 residues before or after the proposed *His* ligands (Saraste 1984; Widger et al. 1984; Hauska et al. 1988). Although the actual ionization state of this residue in the membrane proteins is currently unknown, the low frequencies observed for the ν_{11} mode of reduced membrane cyt *b* (1 529–1 536 cm^{-1}) could therefore correspond to H-bonding interaction of at least one of the *His* ligands e.g. with a nearby basic residue.

Iron oxidation and imidazole deprotonation

It is well known that the acidity of the N_1-H groups of imidazoles increases upon complexation of a metal atom at the N_3 nitrogen (Sundberg and Martin 1974). pK_a values of 10.3–10.5 have been determined for ImH complexes of oxidized myoglobin, hemoglobin and of FePP dimethylester while free ImH in water has a pK_a value of 14.2–14.5 (Mohr et al. 1967; Yagil 1967a; Sundberg and Martin 1974). The pK_a values obtained in the present work for Fe(II)PP$(ImH)_2$ in aqueous CTABr solutions (13.0 and 14.1), relative to those obtained for Fe(III)PP$(ImH)_2$ (9.0 and 10.8), demonstrate the strong influence of the oxidation state of the metal atom on the strength of the N_1-H bonds of bound imidazoles. The formal positive charge of Fe(III)PP$(ImH)_2$, relative to the null charge of Fe(II)PP$(ImH)_2$, certainly has a strong electron withdrawing effect on these bonds.

From these large pK_a differences (3.3–4.0 units), one could envision a model by which a hypothetical cytochrome bearing two axial histidylimidazoles (*HisH*) could be both an electron and a proton carrier. Since the deprotonation of axial imidazoles complexed to an iron-porphyrin stabilizes the ferric oxidation state and drops the potential of the metal atom by as much as 700 mV (Quinn et al. 1983), this hypothetical cytochrome could be operative under at least two of the following three redox couples: Fe(III)PP$(HisH)_2$/Fe(II)PP$(HisH)_2$, Fe(III)PP$(HisH)(His^-)$/Fe(II)PP$(HisH)(His^-)$ and Fe(III)PP$(His^-)_2$/Fe(II)PP$(His^-)_2$, corresponding to high (HP), low (LP) and very low (VLP) potentials, respectively (Fig. 10). Although the pK_a values which we measured in the present study are not physiological, particular environmental conditions, such as proximity of buried polar or charged groups of the protein and hydrophobicity of the heme pocket, may lower them by several units. Ionizations of protein histidylimidazole bound to a ferriheme have actually been characterized between pH 6.5 and 9.0 in oxidized leghemoglobin, cyt *c'* and cyt b_{562} (Weber 1982; Sievers et al. 1983; Moore et al. 1985). Therefore, assuming that the difference of 3–4 pK_a units between Fe(III)PP$(ImH)_2$ and Fe(II)PP$(ImH)_2$ is roughly kept constant between the oxidized and the reduced forms of heme in hemoproteins, the mono- and bis-(histidine) complexes of natural iron-porphyrins are potentially able to transfer one or two proton(s) per electron under favorable environmental conditions. This is made possible by the good H^+-donor abilities of the mono- and bis-(ImH) complexes of the oxidized heme and the very high H^+-acceptor abilities of the mono- and bis-(Im^-) complexes of the reduced heme (Fig. 10).

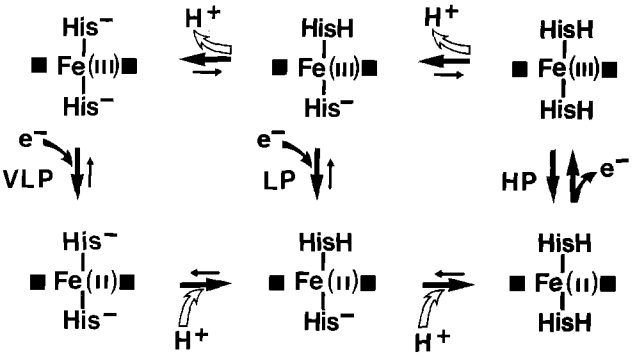

Fig. 10. Scheme of a plausible coupling of electron and proton transfers in a cytochrome containing two histidylimidazoles as heme ligands; VLP, very low potential; LP, low potential; HP, high potential

Coupling of electron and proton transfers in membrane cytochromes b

No cytochrome is yet known which would directly transfer both electrons and protons from its heme and its axial histidylimidazole(s). However, several *b*-type cytochromes are more or less clearly involved in H^+ translocations coupled to electron transfers in mitochondrial (b_{560}, b_{562}, b_{566}), chloroplast (b_{559}, b_{563} or b_6), bacterial (b_{561}, b_{565}), cytoplasmic (b_{558}) or granule (b_{561}) membranes (Wikström 1973; Hauska et al. 1983; Degli Esposti 1989).

The diheme cytochromes *b* of mitochondrial and bacterial *b c* complexes and of chloroplast b_6f complexes present several similarities concerning both functional and molecular aspects. As already mentioned, spatial models predict an assembly of 8–9 membrane-spanning α-helices with the hemes confined between two of these, in planes perpendicular to, and near to the opposite sides of, the membrane (Saraste 1984; Widger et al. 1984; Cramer et al. 1987). The heme locations within a hydrophobic protein core and close to the inner and outer membrane faces therefore appear particularly adapted for efficient transmembrane electron transfers. Moreover, these cytochromes are involved in H^+ translocations through a *Q* cycle, a *b* cycle and/or proton-pump mechanisms (Mitchell 1976; Cramer and Whitmarsh 1977; Wikström et al. 1981; Rich 1984). Although these preceding cyclic pathways exclude any direct participation of hemes in the

proton transfers, their *His* ligands could, however, be privileged sites for a redox control of proton translocation. From the acid-base titrations performed in this study, we can suggest that a histidyl residue bound to an oxidized heme could participate in a proton transfer forming, at least transiently during the turnover of cyt *b*, a histidylimidazolate ligand. As in the case of the interaction of bound Im^- with the head groups of micellar trimethylammonium ions, the formation and stabilization of a histidylimidazolate group require electrostatic interactions with a neighbouring, positively charged group provided by the protein. Sequence data on membrane cyt *b* locate four largely conserved *Arg* residues in close vicinity to the *His* residues likely constituting the heme ligands (Saraste 1984; Widger et al. 1984; Hauska et al. 1988). In some cases, one of these Arg residues is replaced by another basic residue, *His* or *Lys* (Hauska et al. 1988). Crystallographic data available for various *b*- and *c*-type cytochromes reveal that the heme-axial ligands complexes are often within potential interacting range with a nearby guanidium group of an *Arg* residue. Although this situation does not necessarily imply an actual interaction (see Mathews et al. 1972a, b; Xia and Mathews 1990), this positive side chain may serve to the neutralization of a heme propionate as observed in several cytochromes *c* and c_2 (Moore et al. 1984). A positively charged *Arg* side chain also may stabilize the anionic form of a *His* heme ligand in cyt *c'*, *cyt* c_{556} or cyt b_{562} (Moore et al. 1985).

It has been proposed that, in mitochondrial *cyt b* and chloroplast b_6, two *Arg* residues may neutralize the two propionate groups of each heme (Cramer et al. 1987; Hauska et al. 1988). Because the orientations of peripheral heme groups are actually unknown, we may alternatively hypothesize that at least one of these *Arg* residues could interact with a heme ligand possessing an imidazolate character. In addition, a deprotonation of a *His* side chain and its involvement in an ionic interaction with an *Arg* side chain might result into imidazole ring rotations, which might further propagate into larger conformational changes in the vicinity of the ferriheme pockets and along the transmembrane α-helices (Williams 1989). In this hypothesis, we may further consider a series of ion pairs histidinate$^-$(axial *His*)-guanidium$^+$(*Arg*)-propionate$^-$(heme), which would be stabilized by hydrogen and ionic interactions when the heme is oxidized and would be suppressed by *His* protonation when the heme is reduced. This hypothetical triad could hence act as a redox-dependent gate for H^+ entry or exit. A part of the testing of the above models resides in further studies on the ferric forms of mitochondrial and chloroplast cyt *b*.

Another example of cytochrome presenting some interesting analogies with the model proposed in Fig. 10 is constituted by chloroplast cyt b_{559}. Indeed, this hemoprotein *i)* is both an electron carrier and a proton carrier (Cramer and Whitmarsh 1977); *ii)* its sequence suggests that two *His*, provided by two polypeptides arranged in transmembrane α-helices, should be the heme ligands (Herrman et al. 1984); *iii)* it exhibits at least two different redox forms (Rich and Bendall 1980); *iv)* the redox potential of the HP form is in the +320–395 mV range and

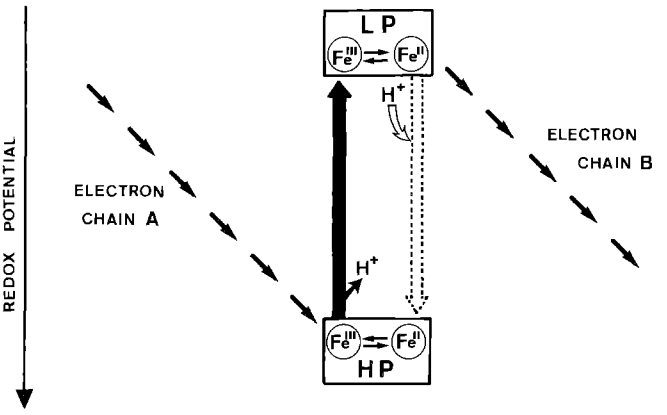

Fig. 11. Scheme of redox-acid-base energy transduction between two electron chains; LP, low potential; HP, high potential

is pH-independent, while that of the LP form is pH-independent above 7.6 (+140 mV) but becomes pH-sensitive below this pH (Bendall 1982; Ortega et al. 1988). The oxidized form of cyt b_{559} has been characterized by EPR spectroscopy (Bergström and Vänngard 1982; Babcock et al. 1985). The HP and LP forms were identified as low spin hemes with g_z values of 3.08 and 2.94, respectively. This small decrease of the g_z factor (−0.14) when going from the HP to the LP form was interpreted as corresponding to a decrease in the dihedral angle of axial imidazole rings (Babcock et al. 1985). This modest structural change however appears insufficient to account for all the properties of cyt b_{559} (Walker et al. 1986). Deprotonation of both axial imidazoles in ferric heme compounds generally decrease the g_z value by ca. 0.2 (Peisach et al. 1973; Yoshimura and Ozaki 1984). Therefore, the 3.08–2.94 g_z change of oxidized cyt b_{559} could originate from a deprotonation of one of the histidylimidazole ligands. As for mitochondrial cyt *b* and chloroplast cyt b_6, an *Arg* residue positioned five residues before the proposed *His* ligands (Herrmann et al. 1984), might stabilize this anionic form in the LP oxidized cyt b_{559}.

The lowering of heme redox potential upon histidylimidazole ionization could also play a key role in the regulation of electron flow toward different electron transfer chains. A reduced LP form of a cytochrome could serve as an electron donor to an electron transfer chain while its oxidized HP form could act as an electron acceptor from another electron chain; this cytochrome would thus behave as a transducer of redox energy into acid-base energy between two electron transfer pathways (Fig. 11). Cyt b_{559} again constitutes a good candidate for involving such a mechanism. In addition to its redox and acid-base properties described above, it is indeed functionally located between the reduced side of photosystem II and the oxidized side of photosystem I (Cramer and Whitmarsh 1977).

Acknowledgements. We gratefully acknowledge helpful discussions with Dr. T.A. Mattioli.

References

Abe M, Kitagawa T, Kyogoku Y (1978) Resonance Raman spectra of octaethylporphyrinato-Ni(II) and meso-deuterated and ^{15}N-

substituted derivatives. II. A normal coordinate analysis. J Chem Phys 69:4526–4534

Adar F (1975) Resonance Raman spectra of cytochrome b_5 and its mesoheme and dueteroheme modifications. Arch Biochem Biophys 170:644–650

Adar F, Erecinska M (1974) Resonance Raman spectra of the *b*- and *c*-type cytochromes of succinate-cytochrome *c* reductase. Arch Biochem Biophys 165:570–580

Adar F, Dixit SN, Erecinska M (1981) Resonance Raman spectra of cytochromes *c* and *b* in *Paracoccus denitrificans* membranes: evidence for heme-heme interactions. Biochemistry 20:7528–7531

Babcock GT, Widger WR, Cramer WA, Oertling WA, Metz JG (1985) Axial ligands of chloroplast cytochrome *b*-559: identification and requirement for a heme-cross-linked polypeptide structure. Biochemistry 24:3638–3645

Bendall DS (1982) Photosynthetic cytochromes of oxygenic organisms. Biochim Biophys Acta 683:119–151

Bergström J, Vänngard T (1982) EPR signals and orientation of cytochromes in the spinach chloroplast thylakoid membrane. Biochim Biophys Acta 682:452–456

Boldt NJ, Goodwill KE, Bocian DF (1988) Comparison of back-bonding in osmium(II) versus ion(II) octaethylporphyrin via resonance Raman spectroscopy. Inorg Chem 27:1188–1191

Brochette P, Zemb T, Mathis P, Pileni M-P (1987) Photoelectron transfer from chlorophyll to viologens in reverse micelles. Unusual interfacial effect on the reaction. J Phys Chem 91:1444–1450

Choi S, Spiro TG (1983) Out-of-plane deformation modes in the resonance Raman spectra of metalloporphyrins and heme proteins. J Am Chem Soc 105:3683–3692

Choi S, Spiro TG, Langry KC, Smith KM, Budd LD, La Mar GN (1982) Structural correlations and vinyl influences in resonance Raman spectra of protoheme complexes and proteins. J Am Chem Soc 104:4345–4351

Collins DM, Countryman R, Hoard JL (1972) Stereochemistry of low-spin iron porphyrins. I. bis(imidazole)-$\alpha,\beta,\gamma,\delta$-tetraphenylporphyrinato-iron(III) chloride. J Am Chem Soc 94:2066–2072

Cramer WA, Whitmarsh J (1977) Photosynthetic cytochromes. Annu Rev Plant Physiol 28:133–172

Cramer WA, Black MT, Widger WR, Girvin ME (1987) Structure and function of photosynthetic cytochrome b/c_1 and b_6/f complexes. In: Barber J (ed) The light reactions. Elsevier, Amsterdam, pp 447–493

Cross PC, Van Vleck JH (1933) Molecular vibrations of three particle system with special applications to the ethyl halides and ethyl alcohol. J Chem Phys 1:350–356

Davies TH (1973) Ferriprotoporphyrin and its imidazole complex in aqueous ethanolic solution. Biochim Biophys Acta 329:108–117

Degli Esposti M (1989) Prediction and comparison of the haem-binding sites in membrane haemoproteins. Biochim Biophys Acta 977:249–265

Demoulin D, Pullman A (1978) An ab initio theoretical study of the binding of Zn^{II} with biologically significant ligands: CO_2, H_2O, OH^-, imidazole, and imidazolate. Theor Chim Acta (Berlin) 49:161–181

Desbois A, Lutz M (1981) Low-frequency vibrations of ferroprotoporphyrin-substituted imidazole complexes. A resonance Raman study. Biochim Biophys Acta 671:168–176

Desbois A, Lutz M (1983) On the assignment of the 190–280 cm^{-1} resonance Raman bands of hemoproteins and models. In: Schnek AG, Paul C (eds) Hemoglobin. Editions de l'Université de Bruxelles, pp 285–298

Desbois A, Lutz M, Banerjee R (1979) Low-frequency vibrations in resonance Raman spectra of horse heart myoglobin. Iron-ligand and iron-nitrogen vibrational modes. Biochemistry 18:1510–1518

Desbois A, Henry Y, Lutz M (1984a) Influence of peripheral substituents on the resonance Raman spectra of ferroporphyrin-2-methylimidazole complexes. Biochim Biophys Acta 785:148–160

Desbois A, Mazza G, Stetzkowski F, Lutz M (1984b) Resonance Raman spectroscopy of protoheme-protein interactions in oxygen-carrying hemoproteins and in peroxidases. Biochim Biophys Acta 785:161–176

Desbois A, Tegoni M, Gervais M, Lutz M (1989) Flavin and heme structures in lactate : cytochrome *c* oxidoreductase: a resonance Raman study. Biochemistry 28:8011–8022

Doeff MM, Sweigart DA, O'Brien P (1983) Hydrogen bonding from coordinated imidazole in ferric porphyrin complexes. Effect on the Fe(III)/Fe(II) reduction potential. Inorg Chem 22:851–852

Falk JE (1964) Redox behaviour of metalloporphyrins. In: Porphyrins and metalloporphyrins, vol 2. BBA Library. Elsevier, Amsterdam, pp 67–71

Gallagher WA, Elliott WB (1973) Ligand-binding in porphyrin systems. Ann NY Acad Sci 206:463–482

Harbury HA, Cronin JR, Fanger MW, Hettinger TP, Murphy AJ, Myer YP, Vinogradov SN (1965) Complex formation between methionine and a heme peptide from cytochrome *c*. Proc Natl Acad Sci USA 54:1658–1664

Hauska G, Hurt E, Gabellini N, Lockau W (1983) Comparative aspects of quinol-cytochrome *c*/plastocyanin oxidoreductases. Biochim Biophys Acta 726:97–133

Hauska G, Nitschke W, Herrmann RG (1988) Amino acid identities in the three redox center-carrying polypeptides of cytochrome $b\,c_1/b_6f$ complexes. J Bioenerg Biomembr 20:211–228

Herrmann RG, Alt J, Schiller B, Widger WR, Cramer WA (1984) Nucleotide sequence of the gene for apocytochrome *b*-559 on the spinach plastid chromosome: implications for the structure of the membrane protein. FEBS Lett 176:239–244

Herschbach DR, Laurie VW (1961) Anharmonic potential constants and their dependence upon bond length. J Chem Phys 35:458–463

Hobbs DD, Kriauciunas A, Güner S, Knaff DB, Ondrias MR (1990) Resonance Raman spectroscopy of cytochrome $b\,c_1$ complexes from *Rhodospirillum rubrum*: initial characterization and reductive titrations. Biochim Biophys Acta 1018:47–54

Kassner RJ (1972) Effects of nonpolar environments on the redox potentials of heme complexes. Proc Natl Acad Sci USA 69:2263–2267

Kim D, Su YO, Spiro TG (1986) Back-bonding in ruthenium porphyrins as monitored by resonance Raman spectroscopy. Inorg Chem 25:3993–3997

Kitagawa T, Ozaki Y (1987) Infrared and Raman spectra of metalloporphyrins. Structure Bonding 64:71–114

Kitagawa T, Sugiyama T, Yamano T (1982) Differences in stability against thermal unfolding between trypsin- and detergent-solubilized cytochrome b_5 and structural changes in the heme vicinity upon the transition: resonance Raman and absorption study. Biochemistry 21:1680–1686

Mathews FS, Argos P, Levine M (1972a) The structure of cytochrome b_5 at 2.0 Å resolution. Cold Spring Harbor Symp Quant Biol 36:387–395

Mathews FS, Levine M, Argos P (1972b) Three-dimensional Fourier synthesis of calf liver cytochrome b_5 at 2.8 Å resolution. J Mol Biol 64:440–464

Menger FM, Doll DW (1984) On the structure of micelles. J Am Chem Soc 106:1109–1113

Meot-Ner M (1988) Models for strong interactions in proteins and enzymes. 2. interactions of ions with the peptide link and with imidazole. J Am Chem Soc 110:3075–3080

Mitchell P (1976) Possible molecular mechanisms of the protonmotive function of cytochrome systems. J Theor Biol 62:327–367

Mitchell ML, Li XY, Kincaid JR, Spiro TG (1987) Axial ligand and out-of-plane vibrations for bis(imidazolyl)heme: Raman and infrared ^{54}Fe, ^{15}N and ^{2}H isotope shifts and normal coordinate calculations. J Phys Chem 91:4690–4696

Mohr P, Scheler W, Schumann H, Müller K (1967) Ligand-protein interactions in imidazole and 1,2,3-triazole complexes of methaemoglobin from *Chironomus plumosus*. Eur J Biochem 3:158–163

Momenteau M (1973) The physical chemistry of hemes and hemopeptides. I. Physicochemical properties and reduction of chlorodeuterohemin in organic solvent. Biochim Biophys Acta 304:814–827

Moore GR, Harris DE, Leitch FA, Pettigrew GW (1984) Characterization of ionisations that influence the redox potential of mitochondrial cytochrome *c* and photosynthetic bacterial cytochromes c_2. Biochim Biophys Acta 764:331–342

Moore GR, Williams RJP, Peterson J, Thomson AJ, Mathew FS (1985) A spectroscopic investigation of the structure and redox properties of *Escherichia coli* cytochrome *b*-562. Biochim Biophys Acta 829:83–96

Nappa M, Valentine JS, Snyder PA (1977) Imidazolate complexes of ferric porphyrins. J Am Chem Soc 99:5799–5800

Ortega JM, Hervas M, Losada M (1988) Redox and acid-base characterization of cytochrome *b*-559 in photosystem II particles. Eur J Biochem 171:449–455

Ozaki Y, Iriyama K, Ogoshi H, Ochiai T, Kitagawa T (1986) Resonance Raman characterization of iron-chlorin complexes in various spin, oxidation, and ligation state. I. Comparative study with corresponding iron-porphyrin complexes. J Phys Chem 90:6105–6112

Paleos CM (1985) Polymerization in organized systems. Chem Soc Rev 14:45–67

Parthasarathi N, Hansen C, Yamagushi S, Spiro TG (1987) Metalloporphyrin core size resonance Raman marker bands revisited: implications for the interpretation of hemoglobin photoproduct Raman frequencies. J Am Chem Soc 109:3865–3871

Peisach J, Mims WB (1977) Linear electric field in electron paramagnetic resonance for two bisimidazole-heme complexes, model compounds for B and H hemichromes of hemoglobin and for cytochrome b_5. Biochemistry 16:2795–2799

Peisach J, Blumberg WE, Adler A (1973) Electron paramagnetic resonance studies of iron porphin and chlorin systems. Ann NY Acad Sci 206:310–327

Pierrot M, Haser R, Frey M, Payan F, Astier JP (1982) Crystal structure and electron transfer properties of cytochrome c_3. J Biol Chem 257:14341–14348

Quinn R, Nappa M, Valentine JS (1982) New five- and six-coordinate imidazole and imidazolate complexes of ferric tetraphenylporphyrin. J Am Chem Soc 104:2588–2595

Quinn R, Strouse CE, Valentine JS (1983) Crystal structure and properties of a potassium cryptate of bis(4-methylimidazolato)(tetraphenylporphinato)iron(III). Inorg Chem 22:3934–3940

Quinn R, Mercer-Smith J, Burstyn JN, Valentine JS (1984) Influence of hydrogen bonding on the properties of iron porphyrin imidazole complexes. An internally hydrogen bonded imidazole ligand. J Am Chem Soc 106:4136–4144

Rich PR (1984) Electron and proton transfers through quinone and cytochrome *bc* complexes. Biochim Biophys Acta 768:53–79

Rich PR, Bendall DS (1980) The redox potentials of the *b*-type cytochromes of higher plant chloroplasts. Biochim Biophys Acta 591:153–161

Salemme FR, Freer ST, Xuong NH, Alden RA, Kraut J (1973) The structure of oxidized cytochrome c_2 of *Rhodospirillum rubrum*. J Biol Chem 248:3910–3921

Saraste M (1984) Location of haem-binding sites in the mitochondrial cytochrome *b*. FEBS Lett 166:367–372

Scheidt WR, Gouterman M (1983) Ligands, spin state and geometry in hemes and related metalloporphyrins. In: Lever ABP, Gray HB (eds) Iron porphyrins, part one. Addison-Wesley, London, pp 89–139

Scheidt WR, Osvath SR, Lee YJ (1987) Crystal and molecular structure of bis(imidazole)(meso-tetraphenylporphinato)iron(III) chloride. A classic molecule revisited. J Am Chem Soc 109: 1958–1963

Selensky R, Holten D, Windsor MW, Paine JB, Dolphin D, Gouterman M, Thomas JC (1981) Excitonic interactions in covalently-linked porphyrin dimers. Chem Phys 60:33–46

Sievers G, Gadsby PMA, Peterson J, Thomson AJ (1983) Magnetic circular dichroism spectra of soybean leghaemoglobin *a* at room temperature and 4.2 K. Biochim Biophys Acta 742:637–647

Simplicio J (1972) Hemin monomers in micellar sodium lauryl sulfate. A spectral and equilibrium study with cyanide. Biochemistry 11:2525–2528

Spiro TG (1985) Resonance Raman spectroscopy as a probe of heme protein structure and dynamics. Adv Prot Chem 37:111–159

Spiro TG, Burke JM (1976) Protein control of porphyrin conformation. Comparison of resonance Raman spectra of heme proteins with mesoporphyrin IX analogues. J Am Chem Soc 98:5482–5489

Stellwagen E (1978) Haem exposure as the determinate of oxidation-reduction potential of haem proteins. Nature 275:73–74

Sundberg RJ, Martin RB (1974) Interactions of histidine and other imidazole derivatives with transition metal ions in chemical and biological systems. Chem Rev 74:471–517

Swartz JC, Stanford MA, Moy JN, Hoffman BM, Valentine JS (1979) Kinetics of CO binding to Fe(TPP)(Im) and Fe(TPP)(Im^-): evidence regarding protein control of heme reactivity. J Am Chem Soc 101:3396–3398

Takano T, Dickerson RE (1981) Conformation change of cytochrome *c*. II. Ferricytochrome *c* refinement at 1.8 Å and comparison with the ferrocytochrome structure. J Mol Biol 153:95–115

Valentine JS, Sheridan RP, Allen LC, Kahn PC (1979) Coupling between oxidation state and hydrogen bond conformation in heme protein. Proc Natl Acad Sci USA 76:1009–1013

Walker FA, Huynh BH, Scheidt WR, Osvath SR (1986) Models of the cytochromes *b*. Effect of axial ligand plane orientation on the EPR and Mössbauer spectra of low-spin ferrihemes. J Am Chem Soc 108:5288–5297

Weber PC (1982) Correlations between structural and spectroscopic properties of the high-spin heme protein cytochrome *c'*. Biochemistry 21:5116–5119

Widger WR, Cramer WA, Herrmann RG, Trebst A (1984) Sequence homology and structural similarity between cytochrome *b* of mitochondrial complex III and the chloroplast b_6f complex: position of the cytochrome *b* hemes in the membrane. Proc Natl Acad Sci USA 81:674–678

Wikström M (1973) The different cytochrome *b* components in the respiratory chain of animal mitochondria and their role in electron transport and energy conservation. Biochim Biophys Acta 301:155–193

Wikström M, Krab K, Saraste M (1981) Proton-translocating cytochrome complexes. Ann Rev Biochem 50:623–655

Williams RJP (1989) Electron transfer in biology. Mol Phys 68:1–23

Wilson EB (1939) A method of obtaining the expanded secular equation for the vibration frequencies of a molecule. J Chem Phys 7:1047–1052

Xia Z, Mathews FS (1990) Molecular structure of flavocytochrome b_2 at 2.4 Å resolution. J Mol Biol 212:837–863

Yagil G (1967a) The proton dissociation constant of pyrrole, indole and related compounds. Tetrahedron 23:2855–2861

Yagil G (1967b) The effect of ionic hydration on equilibria and rates in concentrated electrolyte solutions. III. The H_- scale in concentrated hydroxide solutions. J Phys Chem 71:1034–1044

Yoshimura T, Ozaki T (1984) Imidazole, imidazolate, and hydroxide complexes of (protoporphyrin IX)iron(III) and its dimethyl ester as model systems for ferric hemoproteins: electron paramagnetic resonance and electronic spectral study. Arch Biochem Biophys 230:466–482